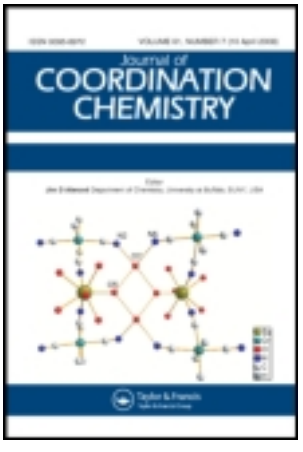

Journal of Coordination Chemistry
Publication details, including instructions for authors and subscription information:
http://www.tandfonline.com/loi/gcoo20

Syntheses, crystal structures, and properties of two macrocyclic dinuclear Ni(II) complexes bearing 2-pyridylmethyl pendant-arms

Q.R. Cheng [a b], J.Z. Chen [a], H. Zhou [b] & Z.Q. Pan [b]
[a] School of Materials Science and Chemical Engineering, China University of Geosciences, Wuhan, P.R. China
[b] Key Laboratory for Green Chemical Process of Ministry of Education, Wuhan Institute of Technology, Wuhan, P.R. China
Published online: 04 Apr 2011.

To cite this article: Q.R. Cheng, J.Z. Chen, H. Zhou & Z.Q. Pan (2011) Syntheses, crystal structures, and properties of two macrocyclic dinuclear Ni(II) complexes bearing 2-pyridylmethyl pendant-arms, Journal of Coordination Chemistry, 64:7, 1139-1152

To link to this article: http://dx.doi.org/10.1080/00958972.2011.563446

Journal of Coordination Chemistry
Vol. 64, No. 7, 10 April 2011, 1139–1152

Syntheses, crystal structures, and properties of two macrocyclic dinuclear Ni(II) complexes bearing 2-pyridylmethyl pendant-arms

Q.R. CHENG†‡, J.Z. CHEN†, H. ZHOU‡ and Z.Q. PAN*‡

†School of Materials Science and Chemical Engineering, China University of Geosciences, Wuhan, P.R. China
‡Key Laboratory for Green Chemical Process of Ministry of Education, Wuhan Institute of Technology, Wuhan, P.R. China

(*Received 15 October 2010; in final form 10 January 2011*)

Two new dinuclear nickel macrocyclic complexes, $[Ni_2(II)L_1(OAc)] \cdot ClO_4 \cdot CH_3OH \cdot 0.5H_2O$ (**1**) and $[Ni_2(II)L_2(OAc)] \cdot CH_3CN \cdot ClO_4 \cdot 0.5H_2O$ (**2**), have been obtained and fully characterized [where H_2L = macrocycle as the [2 + 2] condensation product of 4-X-2,6-diformylphenol (X = CH_3, Cl) and *N*,*N*-bis(2-aminopropyl)-*N*-(2-pyridylmethyl)amine]. The interactions of the complexes with calf thymus-DNA were studied by UV-Vis and CD spectroscopic techniques. The binding constants of **1** and **2** are 1.5×10^5 and $4.9 \times 10^5 (\text{mol L}^{-1})^{-1}$, respectively. The complexes exhibit powerful DNA cleavage activity. The cleavage process occurs *via* an oxidative cleavage and a hydrolytic mechanism for **1**, while the mechanism for **2** was a hydrolytic cleavage. The variable-temperature magnetisms show that there are weak antiferromagnetic couplings between Ni(II) ions in $[Ni_2L(OAc)]^+$, and the cyclic voltammograms of the complexes are also investigated.

Keywords: Macrocyclic complex bearing pendant-arm; Ni(II) complex; Electrochemistry; Magnetism; DNA cleavage activity

1. Introduction

In recent years much effort has been devoted to the preparation and characterization of pendant-arm macrocycles and their metal complexes owing to the fact that the functionalized pendant arms can provide additional donors, enhance stability of complexes, or promote the formation of supramolecular structures with different properties and applications [1, 2]. Furthermore, functionalized pendant-arm macrocyclic complexes have been designed and prepared to mimic the structure and properties of certain metalloenzymes and metalloproteins [3, 4]. Hirohama *et al.* [5] studied the dynamic behavior of $Cu(aneN_3)^{2+}$ and its acridine conjugate bound to DNA, and proved that the complex bearing conjugate pendant-arms could firmly fix on double helical DNA. In previous work, we reported an unsymmetrical bis-furan-2-ylmethy pendant-armed macrocyclic with heterodinuclear Cu(II)Zn(II) complex [6],

*Corresponding author. Email: zhiqpan@163.com

Journal of Coordination Chemistry
ISSN 0095-8972 print/ISSN 1029-0389 online
DOI: 10.1080/00958972.2011.563446

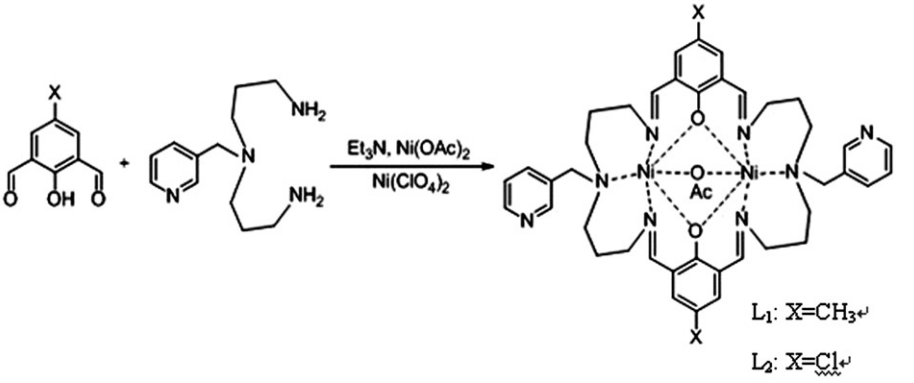

Scheme 1. Synthesis of complexes.

which showed good DNA cleavage activities illustrating that the rigid furan groups in the macrocycle ligand may have synergistic effect in DNA cleavage. We also learned the following: First, the introduction of conjugate pendant groups is expected to increase the conformational rigidity and the stability of the macrocyclic complexes, but it is difficult for conjugate rings with large size to intercalate into the double helical DNA because of the spatial repulsion. Second, the ring size and substituents on the ring are important for DNA cleavage activity [7–11]. Due to the introduction of pyridine pendant groups and the coordination of acetate, macrocycles would be highly twisted to fold into a saddle shape [12, 13] matching with the double helical DNA, for intercalating into the groove of DNA.

In order to establish correlations between the binding structure and the reactivity toward DNA cleavage, and to understand the role of the pyridyl pendant and the benzene ring in DNA cleavage, we designed two new dinuclear nickel macrocyclic complexes with pyridylmethyl pendant-arms and studied the electrochemistry, magnetism, and DNA cleavage activity of the complexes. The route for the synthesis of macrocyclic complexes with pendant arms is shown in scheme 1.

2. Experimental

2.1. *Materials*

Unless otherwise stated, all commercial reagents and solvents were obtained from the commercial provider and used without purification. 2,6-Diformyl 4-*R*-phenol was prepared with high yields by a modified oxidation method [14], and *N*,*N*-bis(2-aminopropyl)-*N*-(2-pyridylmethyl)amine was prepared by the method described in the literature [15].

2.2. *Synthesis of the complexes*

2.2.1. $[Ni_2(II)L_1(OAc)] \cdot ClO_4 \cdot CH_3OH \cdot 0.5H_2O$ (1). To a solution of 2,6-diformyl-4-methylphenol (82.1 mg, 0.5 mmol), $Ni(OAc)_2 \cdot 6H_2O$ (71.2 mg, 0.25 mmol) and

$Ni(ClO_4)_2 \cdot 6H_2O$ (91.4 mg, 0.25 mmol) in acetonitrile–methanol (1 : 1, 30 mL), triethylamine (1 mL) was added. After addition, *N,N*-bis(2-aminopropyl)-*N*-(2-pyridylmethyl)amine (111 mg, 0.5 mmol) in acetonitrile–methanol (1 : 1, 15 mL) was slowly added. The mixture was stirred for 4 h and refluxed for 1 h, then cooled to room temperature and filtered. Green crystals of **1** were obtained by vapor diffusion of diethyl ether into the solution of the complex in acetonitrile–methanol. Yield: 0.221 g, 62%. Anal. Calcd for $C_{90}H_{116}Cl_2N_{16}Ni_4O_{19}$ (%): C, 53.21; H, 5.76; N, 11.03. Found (%): C, 53.19; H, 5.79; N, 11.01. IR(KBr, ν/cm^{-1}): 3049, 2916 (C–H), 1641 (C=N), 1080, 625 (ClO_4^-), 1520, 1414 (COO^-).

2.2.2. $[Ni_2(II)L_2(OAc)] \cdot ClO_4 \cdot CH_3CN \cdot 0.5H_2O$ (2). This compound was prepared by the same procedure as described above except that 2,6-diformyl-4-chlorophenol was used instead of 2,6-diformyl-4-methylphenol. Yield: 0.186 g, 51%. Anal. Calcd for $C_{88}H_{102}Cl_6N_{18}Ni_4O_{17}$ (%): C, 49.59; H, 4.82; N, 11.83. Found (%): C, 49.68; H, 4.71; N, 11.92. IR(KBr, ν/cm^{-1}): 3047, 2913 (C–H), 1638 (C=N), 1076, 628 (ClO_4^-), 1523, 1419 (COO^-).

2.3. *Physical measurements*

IR spectra were recorded on a Vector 22 FT-IR spectrophotometer using KBr disks. Cyclic voltammograms were run on a CHI model 750B electrochemical analyzer in a DMF solution containing tetra(*n*-butyl) ammonium perchlorate (TBAP) as the supporting electrolyte. A three-electrode cell was used, which was equipped with a glassy carbon as the working electrode, a platinum wire as the counter electrode, and a Ag/AgCl electrode as the reference electrode. Scanning rates were in the range of 20–200 mV s^{-1}. The solution was deaerated for 15 min before measurements. The half-wave potentials were calculated approximately from $(E_{pa} + E_{pc})/2$, and the measured error was ±2 mV. Magnetic susceptibility of a crystalline-powdered sample was measured on a SQUID-based sample magnetometer from 2.0–300 K and diamagnetic corrections were made according to Pascal's constants. UV-Vis spectra were recorded on a UV-2450 spectrophotometer. Circular dichroic spectra of DNA were obtained by using a Jasco J-810 spectropolarimeter.

2.4. *X-ray data collection and refinement*

Crystals were measured on a Bruker AXS SMART diffractometer (Mo-Kα radiation monochromator). Data reduction and cell refinement were performed by SMART and SAINT Programs [16]. The structure was solved by direct methods (Bruker SHELXTL) and refined on F^2 by full-matrix least-squares (Bruker SHELXTL) using all unique data [17]. The non-H atoms in the structure were treated as anisotropic. Hydrogen atoms were located geometrically and refined in riding mode.

2.5. *DNA-binding and cleavage experiments*

All the experiments involving the interaction of the complexes with DNA were carried out in Tris–HCl buffer (50 mmol L^{-1} Tris–HCl, pH 7.2) containing 20 mmol L^{-1} NaCl

and 5% DMF at room temperature. A solution of calf thymus-DNA (CT-DNA) in the buffer gave a ratio of UV absorbance at 260 and 280 nm of about 1.89 : 1, indicating DNA sufficiently free from protein [18]. The concentration of CT-DNA was determined from its absorption intensity at 260 nm with a molar extinction coefficient of 6550 $(\text{mol L}^{-1})^{-1}\,\text{cm}^{-1}$ [19].

The electronic spectra of **1** and **2** were monitored both in the absence and presence of CT DNA. Absorption titration experiments were performed by maintaining the metal complex concentration constant (12.5 $\mu\text{mol L}^{-1}$) and varying the nucleic acid concentration (0–75 $\mu\text{mol L}^{-1}$) with reference cell containing DNA alone to nullify the absorbance due to DNA at the measured wavelength. From the absorption titration data, the binding constant was determined using $[\text{DNA}]/E_{\text{ap}} = [\text{DNA}]/E + 1/(K_{\text{b}}E)$ [20], $E_{\text{ap}} = \varepsilon_{\text{a}} - \varepsilon_{\text{f}}$, $E = \varepsilon_{\text{b}} - \varepsilon_{\text{f}}$, where ε_{a}, ε_{f}, and ε_{b} correspond to $A_{\text{obsd}}/[\text{Ni}]$, the extinction coefficient for the free complex, and the extinction coefficient for the complexes in the fully bound form, respectively. A plot of $[\text{DNA}]/(\varepsilon_{\text{a}}-\varepsilon_{\text{f}})$ *versus* [DNA] gives the binding constant K_{b} as the ratio of the slope to the intercept [21].

Cleavage of plasmid DNA was monitored using agarose gel electrophoresis. The reaction was carried out by mixing 2 μL *pBR322* DNA (0.25 $\mu\text{g}\,\mu\text{L}^{-1}$), 4 μL of complex solution (with final concentrations of 3.125, 6.25, 12.5, 25, and 50 $\mu\text{mol L}^{-1}$) and diluting with the Tris–HCl buffer (pH = 7.2) containing 20 mmol L^{-1} NaCl to yield a total volume of 10 μL. The sample was incubated at 37°C, followed by the addition of the loading buffer containing 0.25% bromphenol blue, 50% glycerol, 1% Tris, and the solution was finally loaded on 1% agarose gel containing 0.1 $\mu\text{g mL}^{-1}$ ethidium bromide. Electrophoresis was carried out for 1.5 h at 90 V in TAE buffer (40 mmol L^{-1} Tris, 20 mmol L^{-1} acetic acid, 1 mmol L^{-1} EDTA, pH = 7.4). Bands were visualized by UV light and photographed.

Anaerobic DNA cleavage was carried out by the following steps: all solutions and reaction mixtures were prepared in an argon-filled glovebox. After 3 h incubation period, reactions were stopped in the aerobic environment experiments. All other conditions and procedures were the same as those for aerobic reactions.

3. Results and discussion

3.1. *Synthesis and characterization*

The complexes were obtained by the reaction of 2,6-diformyl-4-X-phenol (X = CH_3, Cl) with *N,N*-bis(2-aminopropyl)-*N*-(2-pyridylmethyl)amine in the presence of $Ni(OAc)_2 \cdot 6H_2O$ and $Ni(ClO_4)_2 \cdot 6H_2O$ in acetonitrile–methanol solution. X-ray structure determinations showed that the two complexes are dinuclear macrocyclic complexes. In IR spectra of the complexes, the sharp C=N stretching vibration bands corresponding to imine groups of the ligand framework are observed at 1641 cm^{-1} for **1** and 1638 cm^{-1} for **2**, indicating that the macrocyclic complexes have been synthesized. The absorption bands of perchlorate are found at 625 and 1081 cm^{-1} for **1** and 628 and 1076 cm^{-1} for **2**, respectively. The similarity of the relative vibration bands of IR in **1** and **2** is in agreement with the comparability of their crystal structures.

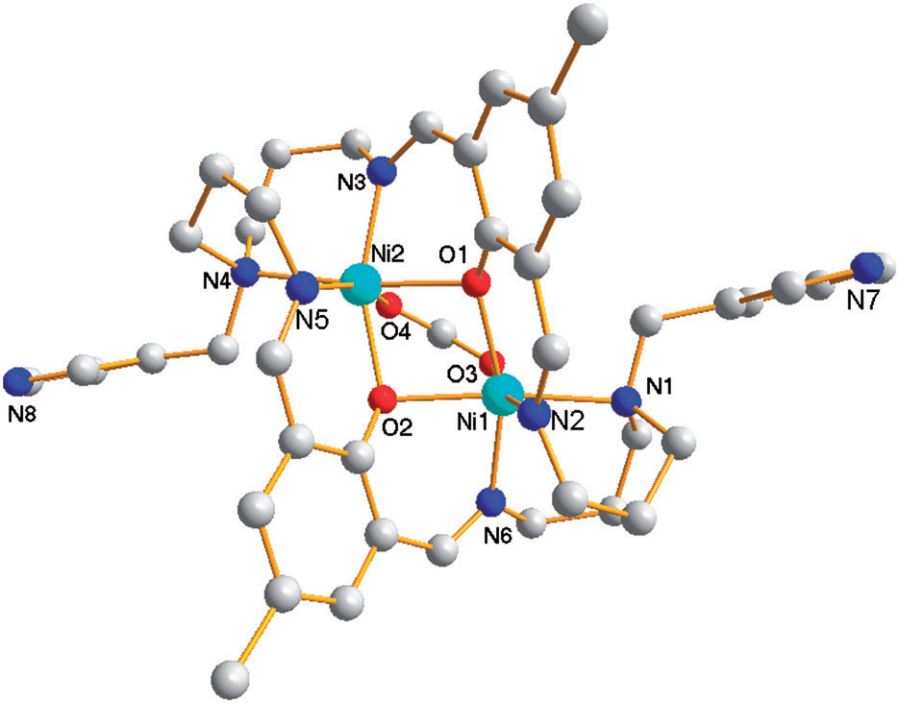

Figure 1. Perspective view of the macrocyclic cation in **1**.

3.2. *Crystal structures*

3.2.1. $[Ni_2(II)L_1(OAc)] \cdot ClO_4 \cdot CH_3OH \cdot 0.5H_2O$ (1). The ORTEP drawing of the macrocyclic cation of **1** is shown in figure 1, together with the numbering scheme. Crystallographic data and details about the data collection are presented in table 1. Selected bond lengths and angles are listed in table 2. The molecular structure of **1** contains a dinuclear cation $[Ni_2L_1(OAc)]^+$, one perchlorate, and an acetonitrile. The ligand is a 30-membered [2 + 2] Schiff-base macrocycle with two pendant-arms being forced to point toward one side of the macrocycle. Two Ni(II) ions were bridged by two μ_2-phenoxy oxygens and one acetate.

The coordination geometry of each Ni(II) can be considered as a distorted octahedron, possibly imposed by steric requirements. The six-coordinate sphere of each metal includes two imine groups, one tertiary nitrogen connected to a pendant arm, two phenolic oxygens, and one oxygen from one acetate. The distance of two Ni(II) ions is 3.152 Å, and the value of the Ni1–O1–Ni2 angle is 99.56(9)°, while the value of the Ni1–O2–Ni2 angle is 98.34(9)°.

Hydrogen-bond interactions play an important role in maintaining the 2-D network of **1** (Supplementary material). Each perchlorate is a H-bond acceptor to link molecules through the following hydrogen-bonding interactions: C1–H1A···O11, C24–H24B···O11, C35–H35···O14 (H···O distances 2.490, 2.550, 2.510 Å and C–H···O angles 170.0, 163.0, 155.0°, respectively). All of the H-bonding acceptors are oxygen of ClO_4^- and the H-bonding donors are carbons of macrocycle and pyridine.

Table 1. Crystallographic data for **1** and **2**.

Empirical formula	$C_{90}H_{116}Cl_2N_{16}Ni_4O_{19}$	$C_{88}H_{102}Cl_6N_{18}Ni_4O_{17}$
Formula weight	1014.86	1065.71
Temperature (K)	291	291
Mo-Kα radiation (Å)	0.71073	0.71073
Crystal system	Triclinic	Monoclinic
Space group	$P\bar{1}$	$P21/c$
Unit cell dimensions (Å, °)		
a	10.6426(10)	14.019(2)
b	12.7541(12)	21.001(3)
c	18.2983(18)	17.147(3)
α	93.252(2)	90
β	95.891(3)	96.957(3)
γ	100.773(2)	90
Volume (Å^3), Z	2419.8(4), 1	5011.1(13), 2
Calculated density (g cm^{-3})	1.393	1.413
Absorption coefficient, μ(Mo-Kα) (mm^{-1})	0.896	0.971
F(000)	1064	2212
Crystal size (mm^3)	$0.20 \times 0.22 \times 0.26$	$0.20 \times 0.22 \times 0.28$
θ range for data collection (°)	2.0–26.0	2.0–26.0
Limiting indices	$-13 \le h \le 11$; $-12 \le k \le 15$; $-229 \le l \le 18$	$-12 \le h \le 17$; $-24 \le k \le 25$; $-19 \le l \le 21$
Tot., uniq. data R(int)	14130, 9320, 0.023	8778, 9827, 0.055
Observed data [$I > 2.0\sigma(I)$]	7067	6729
Nref, Npar	9320, 599	9827, 606
R, wR_2, S	0.0530, 0.1187, 1.05	0.0582, 0.1387, 1.09
Max. and av. shift/error	0.00, 0.00	0.00, 0.00
Min. and max. resd. dens. (eÅ^{-3})	−0.55, 0.64	−0.63, 0.26

3.2.2. $[Ni_2(II)L_2(OAc)] \cdot ClO_4 \cdot CH_3CN \cdot 0.5H_2O$ (2). Except for the different substituent for the phenyl group, the structure of **2** (figure 2) is similar to that of **1**. The distance of two Ni(II) ions is 3.173 Å, and the value of the Ni1–O1–Ni2 angle is 98.63(1)°, while the value of the Ni1–O2–Ni2 angle is 99.22(2)°. Each perchlorate forms a non-classical and weak hydrogen bond (C–H···O) with the molecules (Supplementary material).

3.3. *Electrochemistry*

Electrochemical properties of **1** and **2** were studied by cyclic voltammetry in *N,N*-dimethylformamide (DMF) solution using tetrabutyl ammonium perchlorate (TBAP) as supporting electrolyte from 1.5 to −1.5 V. For **1**, the cyclic voltammogram displays one pair of anodic and cathodic peaks (Supplementary material). The cathodic and anodic peak currents appearing at half-wave potentials ($E_{1/2}$) 0.359 V are unequal. The redox process with half-wave potentials $E_{1/2} = -0.314$ V is attributed to the one-electron transform of Ni(II) Ni(II)/Ni(I) Ni(II), which was pseudo-reversible with $\Delta E = 173$ mV at $\nu = 50$ mV s^{-1}. The value of $i_{pc}/\nu^{1/2}$ remained constant when the scan rate was varied between 50 and 150 mVs^{-1}, indicating that this process was diffusion controlled. With the enhancement of the scan rates, an augmentation in the height of the anodic peak occurs to a greater extent relative to that of the cathodic peak, which reveals that the reduced Ni(II)Ni(I) species is weakly adsorbed on the electrode surface.

Table 2. Selected bond distances (Å) and angles (°) for **1** and **2**.

1		**2**	
Bond lengths (Å)			
Ni1–O1	2.047(2)	Ni1–O1	2.113(3)
Ni1–O2	2.100(2)	Ni1–O2	2.071(3)
Ni1–O3	2.037(2)	Ni1–O3	2.014(3)
Ni1–N1	2.193(3)	Ni1–N1	2.051(3)
Ni1–N2	2.081(3)	Ni1–N5	2.085(3)
Ni1–N6	2.042(3)	Ni1–N6	2.192(3)
Ni2–O1	2.080(2)	Ni2–O1	2.071(3)
Ni2–O2	2.065(2)	Ni2–O2	2.095(3)
Ni2–N3	2.083(3)	Ni2–O4	2.033(3)
Ni2–N4	2.211(3)	Ni2–N2	2.067(3)
		Ni2–N3	2.190(3)
		Ni2–N4	2.091(3)
Bond angles (°)			
O1–Ni1–O2	77.90(9)	O1–Ni1–O2	77.3(1)
O1–Ni1–O3	87.32(9)	O1–Ni1–O3	90.7(1)
O1–Ni1–N1	107.8(1)	O1–Ni1–N1	82.8(1)
O1–Ni1–N2	86.6(1)	O1–Ni1–N5	100.8(1)
O1–Ni1–N6	161.0(1)	O1–Ni1–N6	173.0(1)
O2–Ni1–O3	91.26(9)	O2–Ni1–O3	87.5(1)
O2–Ni1–N1	174.3(1)	O2–Ni1–N1	159.4(1)
O2–Ni1–N2	97.0(1)	O2–Ni1–N5	86.3(1)
O2–Ni1–N6	83.8(1)	O2–Ni1–N6	108.3(1)
O3–Ni1–N1	89.1(1)	O3–Ni1–N1	87.5(1)
O3–Ni1–N2	168.4(1)	O3–Ni1–N5	165.4(1)
O3–Ni1–N6	88.1(1)	O3–Ni1–N6	85.4(1)
N1–Ni1–N2	83.3(1)	N1–Ni1–N5	102.5(1)
N1–Ni1–N6	90.4(1)	N1–Ni1–N6	91.17(1)
N2–Ni1–N6	100.7(1)	N5–Ni1–N6	83.9(1)
O1–Ni2–O2	77.94(9)	O1–Ni2–O2	77.7(1)
O1–Ni2–O4	92.54(9)	O1–Ni2–O4	88.3(1)
O1–Ni2–N3	82.30(9)	O1–Ni2–N2	87.3(1)
O1–Ni2–N4	173.2(1)	O1–Ni2–N3	107.7(1)
O1–Ni2–N5	98.54(9)	O1–Ni2–N4	160.3(1)
O2–Ni2–O4	85.40(9)	O2–Ni2–O4	91.3(1)
O2–Ni2–N3	159.1(1)	O2–Ni2–N2	99.1(1)
O2–Ni2–N4	108.8(1)	O2–Ni2–N3	174.0(1)
O2–Ni2–N5	84.6(1)	O2–Ni2–N4	83.3(1)
O4–Ni2–N3	88.8(1)	O4–Ni2–N2	167.5(1)
O4–Ni2–N4	87.6(1)	O4–Ni2–N3	86.4(1)
O4–Ni2–N5	163.2(1)	O4–Ni2–N4	86.9(1)
N3–Ni2–N4	90.9(1)	N2–Ni2–N3	83.7(1)
N3–Ni2–N5	105.0(1)	N2–Ni2–N4	100.8(1)
N4–Ni2–N5	82.8(1)	N3–Ni2–N4	91.0(1)

For **2**, the cyclic voltammogram displays one pair of anodic and cathodic peaks (Supplementary material S4). When the scan rate was varied between 50 and 150 mVs^{-1}, i_{pa} and i_{pc} increase accordingly, and are in direct proportion to $\nu^{1/2}$, indicating that this process is reversible [22].

3.4. *Magnetic properties*

The magnetic susceptibilities of **1** and **2** were measured on a SQUID magnetometer. Figures 3 and 4 show the $\chi_m T$ *versus* T plot for **1** and **2**, respectively. The $\chi_m T$ values

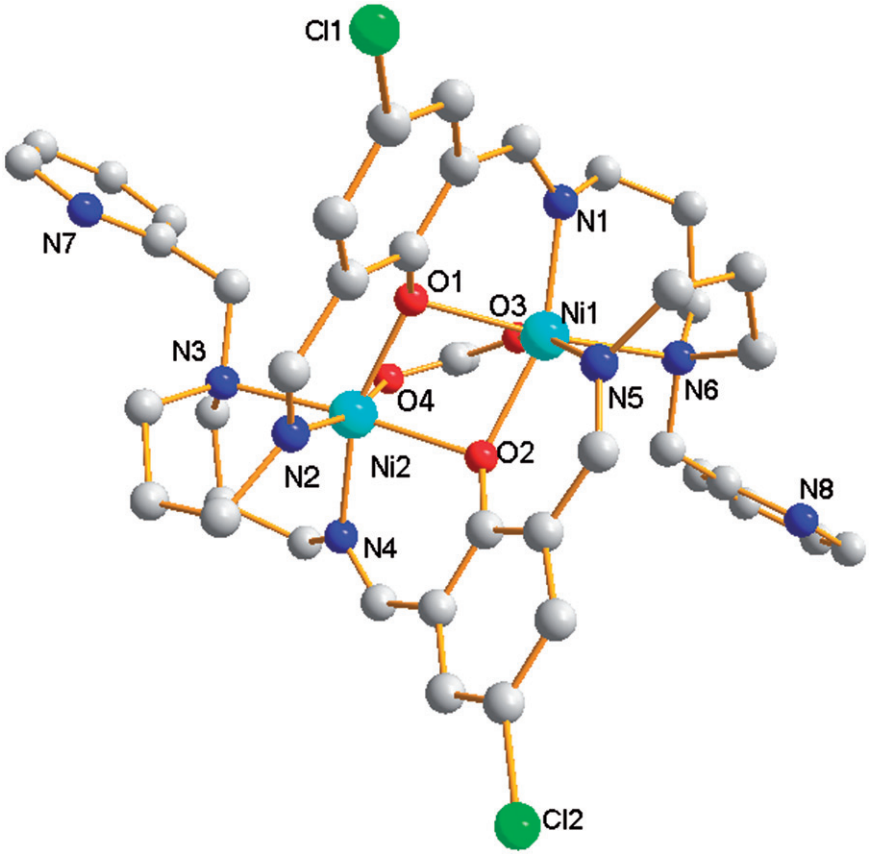

Figure 2. Perspective view of the macrocyclic cation in **2**.

monotonically decreased on cooling, indicating a dominant antiferromagnetic interaction. Magnetic susceptibility data were analyzed using the following isotropic spin Hamiltonian:

$$H = -2JS_1S_2$$
$$\chi_m = \frac{2Ng^2\beta^2}{KT}\frac{e^{(2J/KT)} + 5e^{(6J/KT)}}{1 + 3e^{(2J/KT)} + 5e^{(6J/KT)}} + TIP \quad (1)$$

All the symbols in equation (1) have their usual meaning. J is the exchange coupling parameter and TIP represents metallic impurities. The non-linear least-squares fittings of all experimental $R = \sum[(\chi_M T)_{calc} - (\chi_M T)_{obs}]^2 / \sum(\chi_M T)^2_{obs}$ points gives $g = 2.16$, $J = -1.87\,\mathrm{cm}^{-1}$, TIP = 0.00162 with $R = 2.3 \times 10^{-4}$ for **1** and $g = 2.23$, $J = -2.68\,\mathrm{cm}^{-1}$, TIP = 0.00117 with $R = 2.4 \times 10^{-4}$ for **2** (R is an agreement factor defined as $R = \sum[(\chi_M T)_{calc} - (\chi_M T)_{obs}]^2 / \sum(\chi_M T)^2_{obs}$). The J values indicate a weakly antiferromagnetic interaction between two Ni(II) ions. Similar magnetic behavior was observed for structurally characterized analogous Ni(II) complexes [23–30]. The weak antiferromagnetic behaviors in **1** and **2** are in agreement with the rule reported by

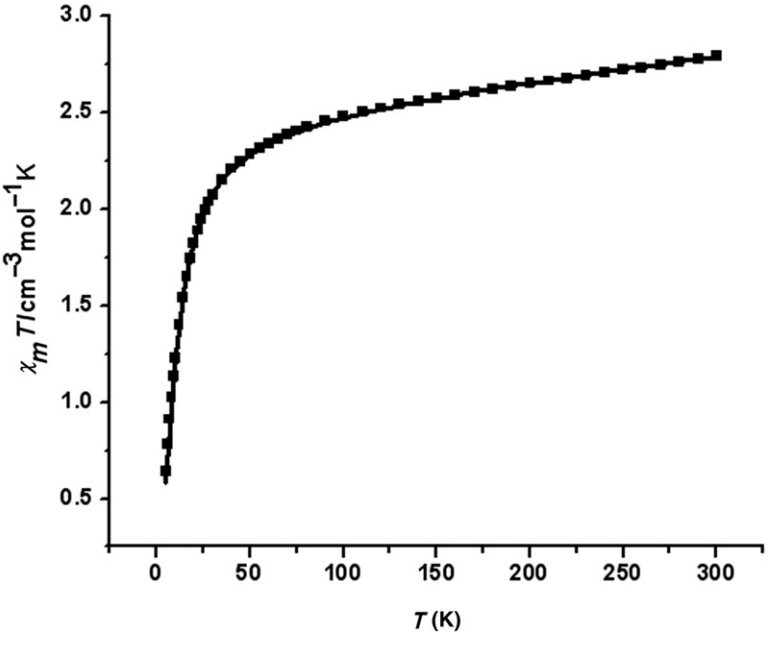

Figure 3. Experimental and calculated plots of $\chi_m T$ *vs.* T for **1**. The solid line represents the best fit curve.

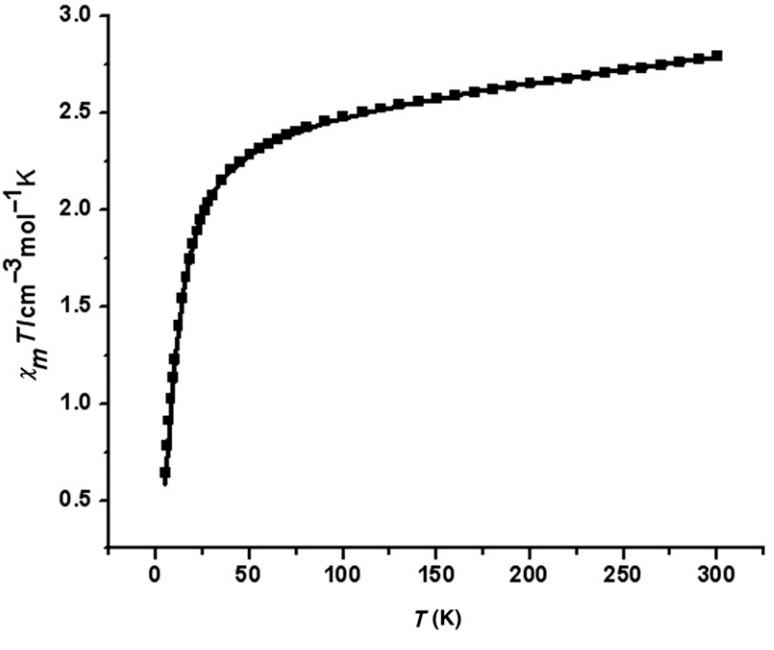

Figure 4. Experimental and calculated plots of $\chi_m T$ *vs.* T for **2**. The solid line represents the best fit curve.

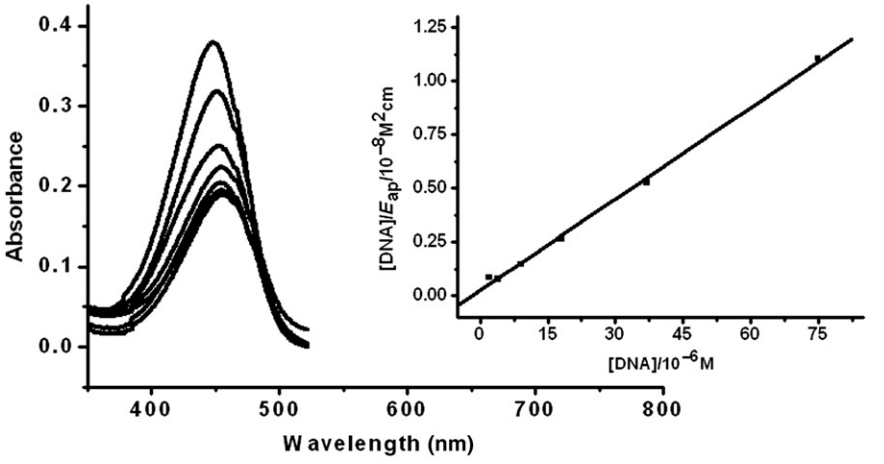

Figure 5. Absorption spectra of **1** in Tris–HCl buffer upon addition of CT-DNA.

Thompson and Nag [31, 32], where the Ni1–O–Ni2 angles are larger than 97°. Similarly, the magnetic behavior of complexes is dependent on the M–N_{azido} bond distance and the M–N_{azido}–M bond angles, such as $[Ni_2^{II}(\mu_{1,1}\text{-}N_3)_2(L)_2(N_3)_2]\cdot H_2O$ (L = 2-[(2-hydroxypropylimino)methyl]phenol), and is dependent on the Ni–O–Ni bond angles, such as $[Ni_2(H_2O)(CH_3OH)(DMF)(L)_2]\cdot H_2O\cdot CH_3OH$ (L = *N,N*-bis(5-ethyl-1,3,4-thiadiazol-2-yl)-2,6-pyridinedicarboxamide) [33, 34].

3.5. *Absorption spectroscopic studies*

Electronic absorption spectroscopy is universally employed to determine the binding characteristics of a metal complex with DNA. The absorption spectra of **1** and **2** in the absence and presence of CT-DNA at different concentrations (0–75 μmol L^{-1}) are shown in figures 5 and 6, respectively. In the UV region, with increasing CT-DNA concentration for **1**, hypochromism in the band at 448.5 nm reaches as high as 50% with a red shift of 7.5 nm at a ratio of [DNA]/[Ni] of 6. The band at 451 nm in **2** shows hypochromism of 49% and a red shift of 7.5 nm under the same experimental conditions. The large hypochromicity and the red shift match the criteria for the intercalative mode [34], so these spectral characteristics suggest that these complexes interact with DNA, most likely through a stacking interaction between the aromatic chromophore and the base pairs of DNA. After intercalating the base pairs of DNA, the π^* orbital of the intercalated ligand can couple with the π orbital of the base pairs, thus decreasing the $\pi-\pi^*$ transition energy, resulting in bathochromism. The intrinsic binding constant K_b is obtained from the ratio of slope to the intercept from plots of [DNA]/$(\varepsilon_a - \varepsilon_f)$ *versus* [DNA]. Intrinsic binding constants K of **1** and **2** were calculated as 1.5×10^5 and 4.9×10^5 $(\text{mol L}^{-1})^{-1}$, respectively. The values of K_b for **1** and **2** are larger than those of other dinuclear Ni(II) complexes [35,36], indicating that macrocycles with a saddle shape could intercalate into the groove of DNA. Furthermore, the results showed that the substituents in benzene ring play an

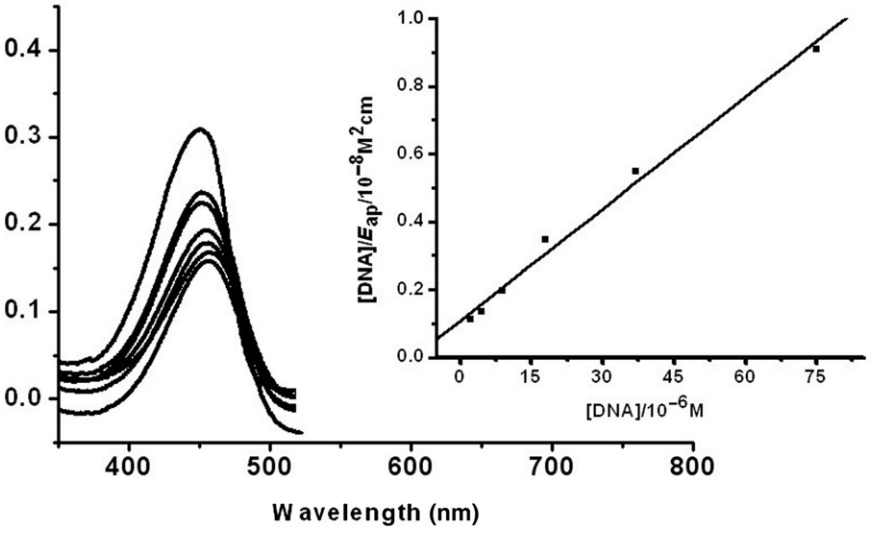

Figure 6. Absorption spectra of **2** in Tris–HCl buffer upon addition of CT-DNA.

important role in DNA cleavage, because the difference between **1** and **2** is the substituent on the benzene ring, methyl for **1** and chlorine for **2**, respectively.

3.6. *CD spectral study*

CD spectroscopy is a useful technique for assessing whether nucleic acids undergo conformational changes as a result of complex formation or changes in the environment. Figure 7 displays the CD spectra of CT-DNA treated with **1** and **2** with a ratio ([complex]/[DNA]) of 0.5. Both the positive (~278 nm) band and the negative (~245 nm) band decreased in intensity in the presence of the complexes. This suggests that **1** and **2** can unwind the DNA helix, leading to the loss of DNA helicity [37, 38]. The larger decrease in the CD band intensity caused by **2** compared to that of **1** at the same concentration implies that **2** is more effective than **1** in perturbing the secondary structure of DNA. From the CD spectroscopy, we conclude that the abilities of the compounds to bind to CT-DNA are in the order **2** > **1**, which is consistent with the results of electronic absorption spectroscopy.

3.7. *Interaction between the complex and plasmid DNA(pBR 322)*

DNA-cleaving ability has been investigated with various concentrations of the complexes at various incubation time intervals. With increasing concentration of the complexes, the intensity of the circular supercoiled DNA band decreases, while that of the nicked band increases. These results (figures 8 and 9) show that the cleavage activity of the complexes was increased with increase in concentration; however, extension of the incubation time has no effect on the cleavage activity of **1**, but has effect on the cleavage activity of **2**.

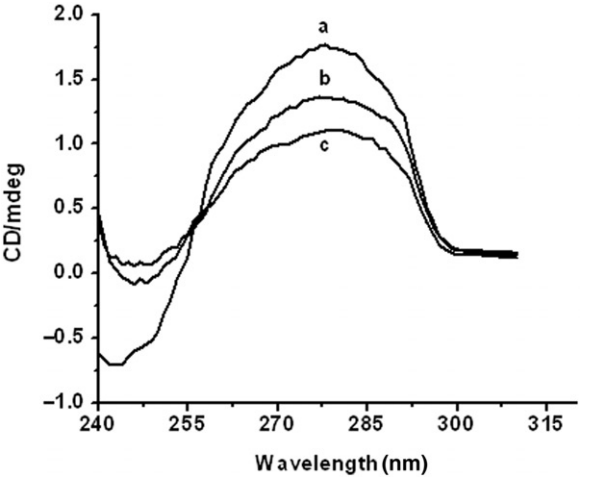

Figure 7. CD spectra of (a) CT-DNA (5.0×10^{-5} mol L^{-1}) and the interaction with **1**(b), **2**(c), at a [compound]/[CT-DNA] ratio of 0.5. All the spectra were recorded in Tris–HCl buffer at pH 7.2.

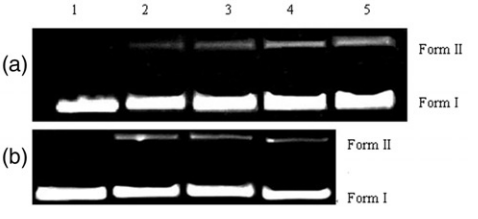

Figure 8. (a) Gel electrophoresis diagram showing the cleavage of *pBR322* DNA (0.25 μg μL^{-1}) by **1** at different concentrations in 50 mmol L^{-1} Tris–HCl/NaCl buffer (pH 7.2) and 37°C for 3 h: Lane 1, DNA control; Lanes 2–5, DNA + **1** (6.25, 12.5, 25, and 50 μmol L^{-1}), respectively. (b) Gel electrophoresis diagram showing the cleavage of *pBR322* DNA (0.25 μg μL^{-1}) by **1** (25 μmol L^{-1}) in 50 mmol L^{-1} Tris–HCl/NaCl buffer (pH 7.2) and 37°C for different incubation time: Lane 1, DNA control; Lanes 2–4, DNA + **1** (25 μmol L^{-1}) for 1, 2, and 3 h.

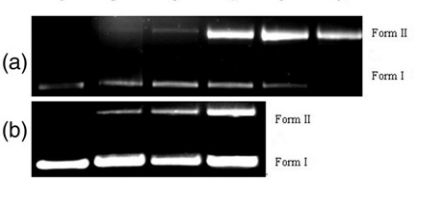

Figure 9. (a) Gel electrophoresis diagram showing the cleavage of *pBR322* DNA (0.25 μg μL^{-1}) by **2** at different concentrations in 50 mmol L^{-1} Tris–HCl/NaCl buffer (pH 7.2) and 37°C for 3 h: Lane 1, DNA control; Lanes 2–6, DNA + **2** (3.125, 6.25, 12.5, 25, and 50 μmol L^{-1}), respectively. (b) Gel electrophoresis diagram showing the cleavage of *pBR322* DNA (0.25 μg μL^{-1}) by **2** (25 μmol L^{-1}) in 50 mmol L^{-1} Tris–HCl/NaCl buffer (pH 7.2) and 37°C for different incubation time: Lane 1, DNA control; Lanes 2–4, DNA + **2** (25 μmol L^{-1}) for 1, 2, and 3 h.

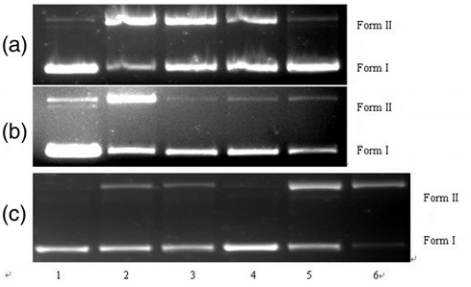

Figure 10. (a) Gel electrophoresis diagram showing the cleavage of *pBR322* DNA (0.25 μg μL^{-1}) by **1** at different scavenging agents in 50 mmol L^{-1} Tris–HCl/NaCl buffer (pH 7.2) and 37°C for 3 h: Lane 1, DNA control; Lane 2, DNA + **1** (12.5 μmol L^{-1}); Lanes 3–5, DNA + **1** (12.5 μmol L^{-1}) + 5 mmol L^{-1} NaN_3; KI; DMSO. (b) Gel electrophoresis diagram showing the cleavage of *pBR322* DNA (0.25 μg μL^{-1}) by **2** at different scavenging agents in 50 mmol L^{-1} Tris–HCl/NaCl buffer (pH 7.2) and 37°C for 3 h: Lane 1, DNA control; Lanes 2–5, DNA + **2** (12.5 μmol L^{-1}) + 5 mmol L^{-1} NaN_3; KI; DMSO; ethanol. Lane 6, DNA + **2** (12.5 μmol L^{-1}). (c) Anaerobic cleavage of *pBR322* DNA (0.25 μg μL^{-1}) by **1** and **2** incubated for 3 h at pH 7.2 and 20°C. Lane 1, DNA control; Lanes 2–3, DNA + **1** (12.5 and 25 μmol L^{-1}, respectively); Lane 4, DNA control; Lanes 5–6, DNA + **2** (25 and 50 μmol L^{-1}, respectively).

To verify the intermediate reactive oxygen species (ROS) in DNA cleavage, we added different scavenging agents to the reaction mixtures. Hydroxyl radical scavengers (5 mmol L^{-1} DMSO), superoxide scavenger (5 mmol L^{-1} KI), and singlet oxygen scavenger (5 mmol L^{-1} NaN_3) were involved in the systems. As shown in figure 10(a), for DNA cleavage by **1** the addition of NaN_3, KI, and DMSO caused a decrease in strand scission. This implies that the mechanism of cleavage by **1** is oxidative cleavage. DNA cleavage by **2** displays a non-oxidizing process due to NaN_3 and KI being ineffective in slowing the cleavage reaction. This implies that a hydrolytic cleavage mechanism occurs under aerobic condition (figure 10b).

As shown in figure 10(c), **1** and **2** have DNA cleavage activity under anaerobic condition, implying that DNA cleavage by **1** occurs by an oxidative cleavage and a hydrolytic mechanism, while DNA cleavage by **2** occurs by a hydrolytic mechanism.

4. Conclusions

Two new dinuclear nickel macrocyclic complexes with pyridylmethyl pendant-arms were prepared and structurally characterized. Cyclic voltammetric experiments of **1** and **2** both showed one pair of anodic and cathodic peaks, and the peak separation ΔE for **1** indicated a quasireversible electrode reaction, while the peak separation ΔE value for **2** indicated a reversible electrode reaction. The magnetic measurements of **1** and **2** revealed a dominant antiferromagnetic interaction between the Ni(II) ions in the macrocyclic unit. Electronic absorption spectroscopy and CD spectra show that the complexes displayed good binding activity with DNA in a non-classical intercalative mode, with benzene rings instead of the pyridyl pendant group which played a role in DNA cleavage. The mechanism for DNA cleavage by **1** included an oxidative cleavage and a hydrolytic cleavage, while the mechanism for **2** was hydrolytic cleavage.

Acknowledgments

We are thankful for the financial support from the National Nature Science Foundation of China (20971102), the Foundation of the Excellent Middle-Young Innovation Group of Education Department of Hubei province (T200802), China.

References

[1] M. Botta. *Eur. J. Inorg. Chem.*, 399 (2000).
[2] K.P. Wainwright. *Adv. Inorg. Chem.*, **52**, 293 (2001).
[3] A. Bianchi, M. Micheloni, P. Paoletti. *Coord. Chem. Rev.*, **110**, 17 (1991).
[4] R.M. Izatt, J.S. Bradshaw, S.A. Nielsen, J.D. Lamb, J.J. Christensen, D. Sen. *Chem. Rev.*, **85**, 271 (1985).
[5] T. Hirohama, H. Arii, M. Chikira. *J. Inorg. Biochem.*, **98**, 1778 (2004).
[6] Y. He, X.H. Wang, H. Zhou, Z.Q. Pan. *Inorg. Chem. Commun.*, **13**, 314 (2010).
[7] E.L. Hegg, K.A. Deal, L.L. Kiessling, J.N. Burstyn. *Inorg. Chem.*, **36**, 1715 (1997).
[8] E.L. Hegg, J.N. Burstyn. *Inorg. Chem.*, **35**, 7474 (1996).
[9] K.A. Deal, J.N. Burstyn. *Inorg. Chem.*, **35**, 2792 (1996).
[10] K.A. Deal, A.C. Hengge, J.N. Burstyn. *J. Am. Chem. Soc.*, **118**, 1713 (1996).
[11] E.L. Hegg, S.H. Mortimore, C.L. Cheung, J.E. Huyett, D.R. Powell, J.N. Burstyn. *Inorg. Chem.*, **38**, 2961 (1999).
[12] J. Kong, H. Zhou, Z.Q. Pan. *Acta Cryst.*, **E64**, m18 (2008).
[13] S. Brooker, P.D. Croucher, T.C. Davidson. *Chem. Commun.*, 2131 (1998).
[14] S. Tanigcuchi. *Bull. Chem. Soc. Jpn.*, **57**, 2683 (1984).
[15] M.L. Turonek, P. Moore, H.J. Class, N.W. Alcock. *J. Chem. Soc., Dalton Trans.*, 3659 (1995).
[16] *SMART* and *SAINT. Area Detector Control and Integration Software*, Siemens Analytical X-ray Systems, Inc., Madison, Wisconsin, USA (1996).
[17] G.M. Sheldrick. *SHELXTL V5.1, Software Reference Manual*, Bruker AXS, Inc., Madison, Wisconsin, USA (1997).
[18] J. Marmur. *J. Mol. Biol.*, **3**, 208 (1961).
[19] A. Wolfe, G.H. Shimer, T. Meehan. *Biochemistry*, **26**, 6392 (1987).
[20] V. Uma, M. Kanthimathi, J. Subramanian. *Biochim. Biophys. Acta*, **1760**, 814 (2006).
[21] A. Wolfe, G.H. Shimer, T. Meehan. *Biochemistry*, **26**, 6392 (1987).
[22] W.L. Mao, Y.Z. Li, Y. Su. *Chin. J. Inorg. Chem.*, **23**, 1201 (2007).
[23] M. Fondo, A.M. Garcia-Deibe, N. Ocampo. *Dalton Trans.*, 4260 (2006).
[24] S. Mandal, V. Balamurugan, F. Lloret. *Inorg. Chem.*, **48**, 7544 (2009).
[25] S.S. Massoud, F.A. Mautner. *Inorg. Chim. Acta*, **361**, 299 (2008).
[26] S.Y. Zhang, Y. Li, W. Li. *Inorg. Chim. Acta*, **362**, 2247 (2009).
[27] R. Ishikawa, A. Fuyuhiro. *J. Mol. Struct.*, **892**, 220 (2008).
[28] M.D. Santana, G. Garcia. *J. Organomet. Chem.*, **693**, 2009 (2008).
[29] X.T. Liu, Q.L. Liu. *J. Mol. Struct.*, **889**, 160 (2008).
[30] X.D. Zheng, L. Jiang, X.L. Feng. *Dalton Trans.*, 6802 (2009).
[31] K.K. Nanda, R. Das, K.L. Thompson, K. Venkatsubramanian, P. Paul. *Inorg. Chem.*, **33**, 1188 (1994).
[32] K.K. Nanda, K.L. Thompson, N.J. Bridson, K. Nag. *J. Chem. Soc., Chem. Commun.*, 1337 (1994).
[33] S.L. Liang, Z.L. Liu, N.R. Liu, C.M. Liu, X.W. Di, J. Zhang. *J. Coord. Chem.*, **63**, 3441 (2010).
[34] X.Q. Shen, Z.F. Li, H.Y. Zhang, Z.J. Li. *J. Coord. Chem.*, **63**, 1720 (2010).
[35] R.F. Pasternack, E.J. Gibbs, J.J. Villafranca. *Biochemistry*, **22**, 2406 (1983).
[36] S. Anbu, M. Kandaswamy, B. Varghese. *Dalton Trans.*, 3823 (2010).
[37] F.R. Pasternack. *Chirality*, **15**, 329 (2003).
[38] K. Karidi, A. Garoufis, N. Hadjiliadis. *Dalton Trans.*, 728 (2005).